AIAA 80-1778R

A New Approach for Active Control of Rotorcraft Vibration

N.K. Gupta*
Integrated Systems, Inc., Palo Alto, Calif.
and
R.W. Du Val†
NASA Ames Research Center, Moffett Field, Calif.

A helicopter vibration controller is designed by optimizing a cost functional, which places a large penalty on fuselage accelerations at vibration frequencies. The solution to the optimal control problem leads to a feedback law where the fuselage accelerations are first filtered by undamped, second-order systems. This vibration control solution has been possible due to a recent extension of the well-known optimal control formulation. The extension allows frequency-dependent penalty functions on states and controls. The design approach is applied to a simulation-derived, nine-degree-of-freedom linear model of the Rotor Systems Research Aircraft in hover. Evaluation on nonlinear simulation with inflexible rotor baldes in hover and forward flight shows essentially complete elimination of vibration. Acceptable blade pitch amplitude is required for closed-loop control. The paper shows feasibility of the approach. Future work will address blade flexibilities and implementation considerations.

Nomenclature

a_w, a_p, a_q	= penalty on states w, p, and q
A_{ls}	= lateral swash-plate deflection
B_{ls}	= longitudinal swash-plate deflection
B	= control penalty
F	= state distribution matrix
LQG	= linear-quadratic-Gaussian control design
LQG ($j\omega$)	= frequency-shaped LQG
MBC	= multiblade coordinates
N	= number of blades
p,q,r	= components of rotational rates
rev	= revolution of the rotor
RSRA	= Rotor Systems Research Aircraft
u,v,w	= components of fuselage speed
u	= control
x	= system state
z	= filter state
β	= flapping angle
$\beta_{r1}, \beta_{r2}, \ldots$	= flapping angle of a particular blade
$\beta_0, \beta_{1c}, \beta_{1s}, \ldots$	= rotor flapping modal states
λ	= root location
ω	= frequency
Ω	= rotor speed
ψ	= blade azimuth angle
ϕ	= fuselage roll angle
σ	= real part of an eigenvalue
θ	= fuselage pitch angle
θ_C	= main rotor collective input
θ_{TR}	= tail rotor collective input
Subscripts	
c	= cosine component
s	= sine component

Introduction

HELICOPTERS encounter significant vibration caused by the variations of rotor blade aerodynamic loads with azimuth angle. Vibration reduces pilot effectiveness and passenger comfort, and increases operating costs and maintenance requirements. Use of helicopters in commercial aviation has been hindered by high vibration levels. The reduction of vibration has, therefore, been of major interest in the helicopter industry.

Helicopter vibration results from: 1) multicyclic main rotor aerodynamic loads, 2) engine turbine, 3) transmission, 4) gear box, and 5) tail rotor. Although vibration signature varies with helicopters, and with location in a helicopter, the pilot station and instrument panel vibration is primarily due to main rotor multicyclic inputs.[1] The vibration level can be 0.5 g or more.

Mass-spring-damper systems are currently used for rotorcraft vibration suppression. These systems are heavy and have limited range of effectiveness. Considerable research has recently been done on "active" techniques, which make direct use of vehicle controls. This paper deals with a new approach to active vibration suppression. Frequency-shaped weighting extensions of optimal control is used.

The paper begins with an analysis of vibration mechanisms and current approaches to active control. The state feedback approach is then discussed. The application of this method is demonstrated using the Rotor Systems Research Aircraft (RSRA) as an example.

The results of a closed-loop nonlinear simulation utilizing this design are presented. Areas for future research are indicated.

Active Control of Rotorcraft Vibrations

Rotor Forces and Control Systems

The forces on a rotor blade are functions of the azimuth angle; therefore, they can be represented as harmonic functions in space. Multiples of N, $N-1$, and $N+1$ cycles per rotor revolution are folded into the steady and one-per-revolution fuselage forces, respectively. This combination produces forces in the fuselage that are multiples of N cycles per rotor revolution (N/rev).[2] In general, the higher the number of blades, the less the vibration transmitted to the fuselage.

Active rotorcraft vibration suppression involves driving the blade pitch to produce incremental aerodynamic forces, which oppose the vibratory force components transmitted to the fuselage. This is accomplished by feathering the blades to minimize the blade forces at the $N-1$, N, and $N+1$ per-revolution frequencies. In most rotorcraft, the blade pitch is

Presented as Paper 80-1778 at the AIAA Guidance and Control Conference, Danvers, Mass., Aug. 11-13, 1980; submitted Oct. 24, 1980; revision received June 2, 1981. This paper is declared a work of the U.S. Government and therefore is in the public domain.

*Research Scientist and President. Member AIAA.
†Research Scientist. Member AIAA.

controlled by a "swashplate" whose orientation determines the phase and amplitude of the constant and one-per-revolution blade-pitch oscillations. Rotorcraft control is implemented through the orientation of the swashplate in the nonrotating fuselage frame. For an N-bladed rotor an N/rev oscillation of the swashplate orientation produces an N, $N-1$, and $N+1$ per-revolution oscillation in the blade pitch, the reverse of the previously described force transformation.

Current Approaches to Active Control

Virtually all current approaches to active control of rotor vibration involves the use of multicyclic inputs. Blade pitch is cycled at $N-1$, N, and $N+1$ per-revolution frequencies, and the phase and amplitude of these multicyclic oscillations are adjusted to minimize blade forces at these frequencies. The required phase and amplitude are obtained from a harmonic analysis of the response to the multicyclic control in a batch mode.[3]

Most multicyclic control investigations involve open-loop control, in which the input-output model is determined experimentally for a steady-state condition. The control is based on this model.[3] Recent investigations[4,5] have proposed an adaptive approach, in which the transmission matrix is identified for slowly varying flight conditions. Although the initial work involved analyzing the input-output model in the rotating frame, some recent studies include harmonic analysis of outputs in the nonrotating (fuselage) frame.[4-6]

The disadvantages of the harmonic analysis approach are the high real-time computation time, and limitations of the input-output model to slowly varying flight conditions.[7]

Vibration Control Using Tuned State Feedback

Modern control theory methods are suitable for multivariable control needed for vibration elimination. A major barrier in the straightforward application of state feedback methods is that the states contain all frequencies. Therefore, a vibration-minimizing controller can aggravate fuselage dynamics and blade structural modes. Recent extensions of linear-quadratic-Gaussian (LQG) methods with capability to place frequency-dependent penalties on states and controls[8] allow vibration control without undesirable side effects. In essence, the technique passes the states, in which vibration is to be suppressed, through a second-order, undamped filter tuned to resonate at the N/rev frequency. The resulting system acts like a phase-locked loop since the control signal is 180 deg out of phase with the vibrations at the filter's resonant frequency of N/rev. The control is therefore able to lock onto vibration phase and amplitude without the use of harmonic analysis. Standard LQG techniques can then be applied to obtain a set of feedback gains that ensure stable control action.[9]

The control law obtained from this procedure is simple to implement because it is, in effect, a constant-gain regulator with filters in the feedback loops. A dynamic model of the rotor-fuselage combination is used in the LQG design procedure so the resulting controller can respond properly to transients. A major advantage of the state-feedback approach is that it allows the application of LQG methods to develop a systematic design of a multi-input, multi-output control system.

All calculations are performed in the nonrotating frame to avoid dynamic transformations, and to work only at N/rev rather than the three frequencies in the rotating frame. Collective and cyclic inputs at N/rev produce rotor harmonics at N, $N-1$, and $N+1$ per rev.

Rotorcraft Model for Vibration Control Design

A model is required to accurately reflect the response of the rotorcraft to both disturbances and controls at vibration frequency. The model is complicated by the many degrees of freedom involved in the rotor dynamics. An articulated rotor, for example, is hinged about two axes to allow both flapping and lead-lag motion. For a five-bladed rotor, this results in ten degrees of freedom (20 states).

The in-flow and the rotor speed constitute at least two additional degrees of freedom, so a combined rotor-fuselage model could require an 18-degree-of-freedom representation. Flexibility would add more states.

Representation of the Rotor

Blade forces are controlled by cyclicly adjusting the blade angle of attack. An instantaneous change in the angle of attack results from a change in the blade pitch angle so the blade pitch directly controls the rotor forces. These forces cause the blades to flap or bend, resulting in a change in the blade angle of attack. The blade pitch, therefore, has both an instantaneous effect on rotor forces and a lagged effect, as the rotor responds dynamically to the pitch input. The natural frequency of the blade dynamics is about one cycle per rotor revolution. At the required control frequencies, the effect of the blade dynamics is important, and must be included in the design of the vibration control system. Quasi-static models are unsuitable for vibration control.

The trick is to develop a time-invariant model for rotor dynamics. The multiblade coordinate (MBC) representation appears useful.[10] This representation provides a dynamic description of a curve passing through the tips of all the rotor blades at an instant of time. For an N-blade rotor, the curve has an N-degree-of-freedom representation. Using this approach, the flapping of the N blades, β_{rj}, is related to the N multiblade coordinates, β_j, for an odd number of blades, by the transformation:

$$\begin{bmatrix} \beta_{r1} \\ \beta_{r2} \\ \vdots \\ \beta_{rN} \end{bmatrix} = \begin{bmatrix} 1 & \cos\psi_1 & \sin\psi_1 & \cdots & \cos\frac{N-1}{2}\psi_1 & \sin\frac{N-1}{2}\psi_1 \\ 1 & \cos\psi_2 & \sin\psi_2 & \cdots & \cos\frac{N-1}{2}\psi_2 & \sin\frac{N-1}{2}\psi_2 \\ \vdots & \vdots & \vdots & & \vdots & \vdots \\ 1 & \cos\psi_N & \sin\psi_N & \cdots & \cos\frac{N-1}{2}\psi_N & \sin\frac{N-1}{2}\psi_N \end{bmatrix} \begin{bmatrix} \beta_0 \\ \beta_{1c} \\ \beta_{1s} \\ \vdots \\ \frac{\beta_{N-1}}{2}c \end{bmatrix} \tag{1}$$

An additional term is required for even-bladed rotors.

Blade dynamics in the rotating frame are represented by a second-order model. If the rotating frame eigenvalues of each blade are $\lambda_r = -\sigma \pm j\omega$, then the N eigenvalues of the MBC representation are[10]

$$\begin{aligned} \lambda_0 &= -\sigma \pm j\omega \\ \lambda_1 &= -\sigma \pm j(\omega \pm \Omega) \\ &\vdots \\ \lambda_{\frac{N-1}{2}} &= -\sigma \pm j(\omega \pm \frac{N-1}{2}\Omega) \end{aligned} \tag{2}$$

For a five-bladed rotor with ω close to 1/rev, the highest frequency root will be at 3/rev, so driving the system at 5/rev should not excite any rigid-body resonances, but may excite aeroelastic modes.

One of the advantages of the MBC representation is that it provides a well-defined dynamic model in a transient while the Fourier representation is only defined under equilibrium conditions. With appropriate sensors, these states could then be estimated and fed back in a flight control system.[11]

Development of Model from Nonlinear Simulation

The model utilized in this analysis is a linear representation of the Rotor System Research Aircraft (RSRA) in hover. The RSRA's five-bladed S-61 rotor is modeled as a three-degree-of-freedom, six-state system, consisting of the coning and first harmonic flapping modes. These modes were found to be the most significant for a 5/rev excitation.[12] The lead-lag motion may also be important, but is neglected to simplify the analysis.

The fuselage dynamics are modeled as a six-degree-of-freedom, eight-state system. The parameters of this linear model were obtained from a least-squares-regression fit of data from a nonlinear, blade-element simulation of the RSRA.[12] The data were obtained by driving the rotor with a 5/rev excitation for an accurate representation of the RSRA at the vibration frequency. The four controls included in the model are the collective (θ_C), longitudinal (B_{1s}), and the lateral (A_{1s}) swashplate deflections, and the tail-rotor collective (θ_{TR}). To simplify the analysis, actuator dynamics are neglected. Actuators have significant lags and attenuations at required control frequencies and must be considered in a practical design.

Vibration Control Design Procedure

A vibration controller is designed for RSRA N/rev pitch, roll, and vertical channel vibration. Let the linearized RSRA state equations be

$$\dot{x} = Fx + Gu \tag{3}$$

$$x^T = [u, w, \theta, q, v, \phi, p, r, \ \beta_0, \beta_{1c}, \beta_{1s}, \dot{\beta}_0, \dot{\beta}_{1c}, \dot{\beta}_{1s}] \tag{4}$$

fuselage states rotor states

$$u^T = [B_{1s}, \theta_C, A_{1s}, \theta_{TR}] \tag{5}$$

If ω is the rotor frequency, the following penalty function is optimized:

$$J = \frac{1}{2}\int_{-\infty}^{\infty} \left[\frac{(5\Omega)^2}{\omega^2 - (5\Omega)^2}\frac{\dot{\omega}^2}{a_\omega^2} + \frac{\dot{q}^2}{a_q^2} + \frac{\dot{p}^2}{a_p^2} + u^T B u\right] d\omega \tag{6}$$

Note that the penalty function is infinite at $\omega = 5\Omega j$ (see Fig. 1 for magnitude and phase). a_ω, a_q, and a_p are the relative weighting parameters. Three tuned filters are required to provide this frequency shaping, one each for vertical acceleration, pitch acceleration, and roll acceleration. The additional states for the vertical acceleration channel take the form

$$\begin{bmatrix} \dot{z}_{1w} \\ \dot{z}_{2w} \end{bmatrix} = \begin{bmatrix} 0 & 1 \\ -(5\Omega)^2 & 0 \end{bmatrix} \begin{bmatrix} z_{1w} \\ z_{2w} \end{bmatrix} + \begin{bmatrix} 0 \\ (5\Omega)^2 \end{bmatrix} \dot{w} \tag{7}$$

Six additional dynamic equations of the following form must therefore be appended to the RSRA model:

$$\dot{z} = Lz + D\dot{x} \tag{8}$$

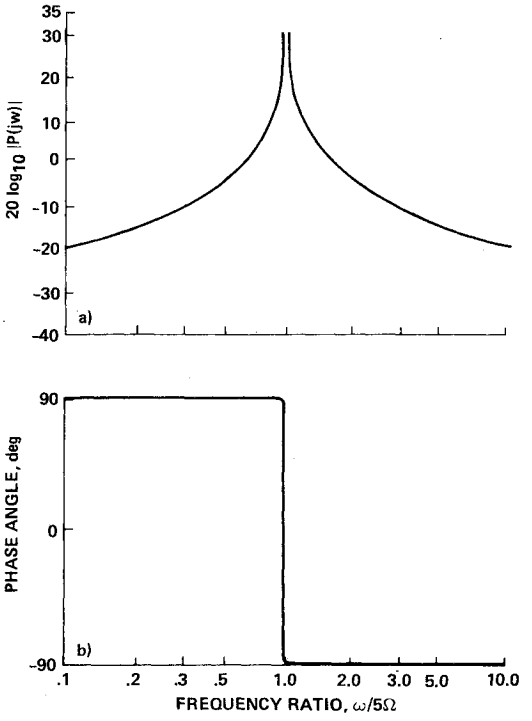

Fig. 1 Frequency-shaped penalty function: a) log magnitude, b) phase plot.

where

$$z^T = [z_{1w}, z_{2w}, z_{1q}, z_{2q}, z_{1p}, z_{2p}] \tag{9}$$

$$L = \left[\begin{array}{cc:cc:cc} 0 & 1 & \multicolumn{2}{c:}{\phi} & \multicolumn{2}{c}{\phi} \\ -(5\Omega)^2 & 0 & \multicolumn{2}{c:}{} & \multicolumn{2}{c}{} \\ \hdashline \multicolumn{2}{c:}{} & 0 & 1 & \multicolumn{2}{c}{} \\ \multicolumn{2}{c:}{\phi} & -(5\Omega)^2 & 0 & \multicolumn{2}{c}{\phi} \\ \hdashline \multicolumn{2}{c:}{} & \multicolumn{2}{c:}{} & 0 & 1 \\ \multicolumn{2}{c:}{\phi} & \multicolumn{2}{c:}{\phi} & -(5\Omega)^2 & 0 \end{array}\right] \tag{10}$$

$$D = \left[\begin{array}{cccccccc:c} 0 & 0 & 0 & 0 & 0 & 0 & 0 & 0 & \\ 0 & (5\Omega)^2 & 0 & 0 & 0 & 0 & 0 & 0 & \\ 0 & 0 & 0 & 0 & 0 & 0 & 0 & 0 & \\ 0 & 0 & 0 & (5\Omega)^2 & 0 & 0 & 0 & 0 & \phi_{6\times 6} \\ 0 & 0 & 0 & 0 & 0 & 0 & 0 & 0 & \\ 0 & 0 & 0 & 0 & 0 & 0 & (5\Omega)^2 & 0 & \end{array}\right] \tag{11}$$

The penalty function may be written in terms of the additional states

$$J = \frac{1}{2}\int_0^\infty \left[\left(\frac{z_{2w}}{a_w}\right)^2 + \left(\frac{z_{2q}}{a_q}\right)^2 + \left(\frac{z_{2p}}{a_p}\right)^2 + u^T B u\right] dt \tag{12}$$

Thus, the frequency-shaping problem with 14 states can be transformed into a 20-state standard LQG problem.

Linear-Quadratic-Gaussian Design

An LQG design of a state feedback controller is performed for various values of a_w, a_q, and a_p with unit control

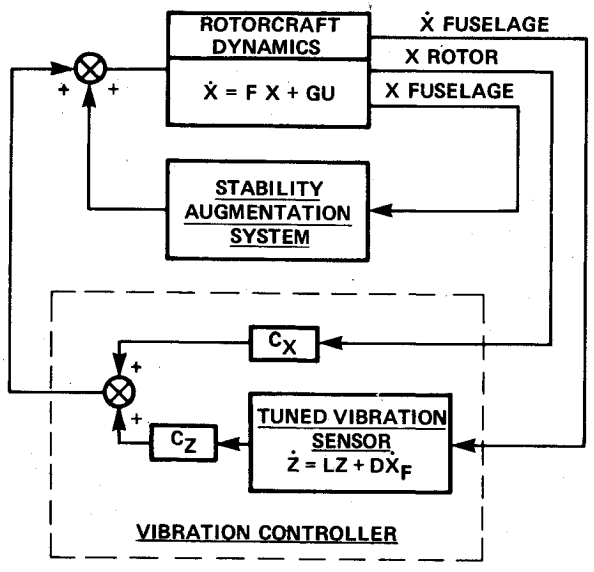

Fig. 2 Schematic representation of system with SAS and vibration controller.

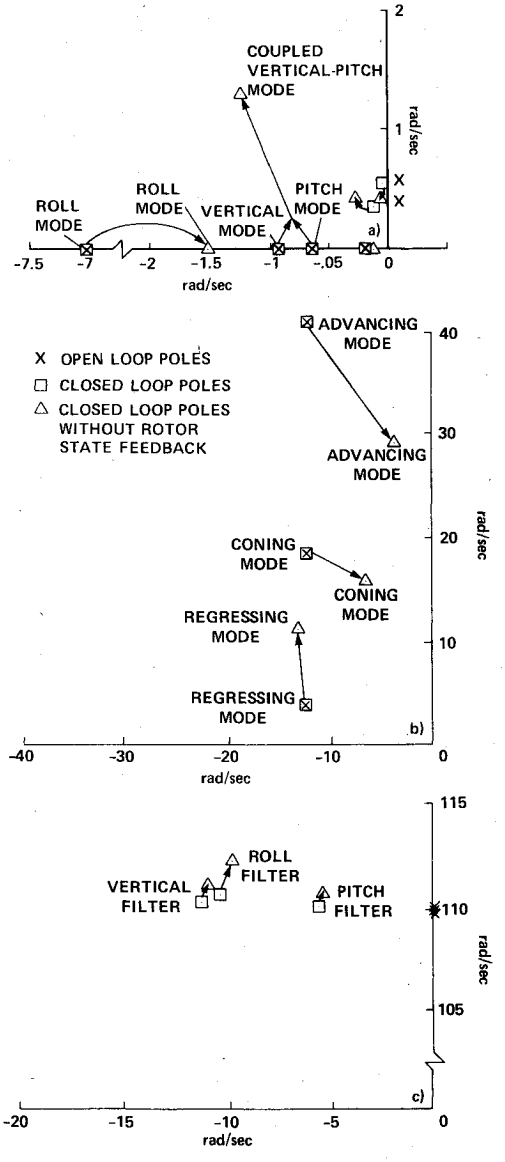

Fig. 3 Roots for open-loop, closed-loop, and closed-loop without rotor-state feedback cases: a) fuselage roots, b) rotor roots, c) filter roots.

weighting.[13] Only eigenvalues of the closed-loop system associated with state z change significantly as the weights are varied. It appears that the vibration controller can be designed independently of any low-frequency autopilot designs.

The response time of the vibration controller is close to the time constant of the closed-loop roots associated with state z. Therefore, the weighting factors are adjusted until all the filters have time constants between 0.1 and 0.25 s, the desired response time of the vibration controller. The final weighting factors and the resulting feedback control gains are given in the Appendix. A schematic representation of the vibration controller is shown in Fig. 2. The fuselage feedback is shown separately to emphasize the independence of the SAS and vibration controller functions.

Effect of Rotor-State Feedback

A controller designed by LQG methods requires feedback of all states. Because rotor-state estimation is not generally available, it was of interest to evaluate the stability of the vibration controller without the use of rotor-state feedback. This was accomplished by obtaining the eigenvalues of the closed-loop system with the rotor-state feedback gains set to zero. Figure 3a shows the fuselage roots for the open-loop, closed-loop, and closed-loop-without-rotor-state feedback cases. Note that the only change in the fuselage roots from the open-loop to the closed-loop case was that the unstable fuselage roots were reflected into the left-half plane, thereby stabilizing the fuselage. Elimination of the rotor-state feedback causes the fuselage roots to change considerably. Two of the real roots, the ones associated with vertical and pitching modes, become complex, and a third real root, associated with the roll mode, is highly destabilized. Research is underway to explain this observation.

Figure 3b shows the rotor roots for these three cases. Again the roots for the open- and closed-loop cases are virtually identical, but by eliminating the rotor-state feedback the level of damping is reduced on all the roots.

Figure 3c shows the roots associated with z for the three cases. The elimination of rotor-state feedback has no significant effect on root locations.

Simulation Results

Nonlinear Simulation

The vibration controller resulting from this design procedure was implemented on a nonlinear, blade-element simulation of the RSRA in hover. The simulation, obtained from the "GENHEL"[14] program, does not include flexibility. Because the vibration controller did not modify the fuselage roots as long as rotor-state feedback was present, it was assumed that a low-frequency fuselage control can be designed independently of the vibration controller. The fuselage feedback was therefore eliminated from the vibration controller, and the conventional RSRA stabilization augmentation system (SAS) was used to stabilize the fuselage in roll, pitch, and yaw. The resulting vibration controller, then, consists of only rotor and state feedback. Since the design did not include actuator dynamics, the controller output was applied directly to the swashplate, effectively simulating perfect actuators. The vibration control algorithm for the tail rotor was not implemented. The z states were implemented with time, as the independent variable. In a practical application, however, blade azimuth would be used as the independent variable to ensure a resonant frequency at N/rev, regardless of changes in rotor speed.

Feedback of Filter and Rotor States

Roll acceleration is shown in Fig. 4a. The relatively small hover vibration levels (about 1.5 deg/s^2) are excited by the cyclic control required to offset the tail rotor thrust in trim. The vibration controller is turned on at 1 s. In the steady state there is no visible trace of the 5/rev vibrations that were

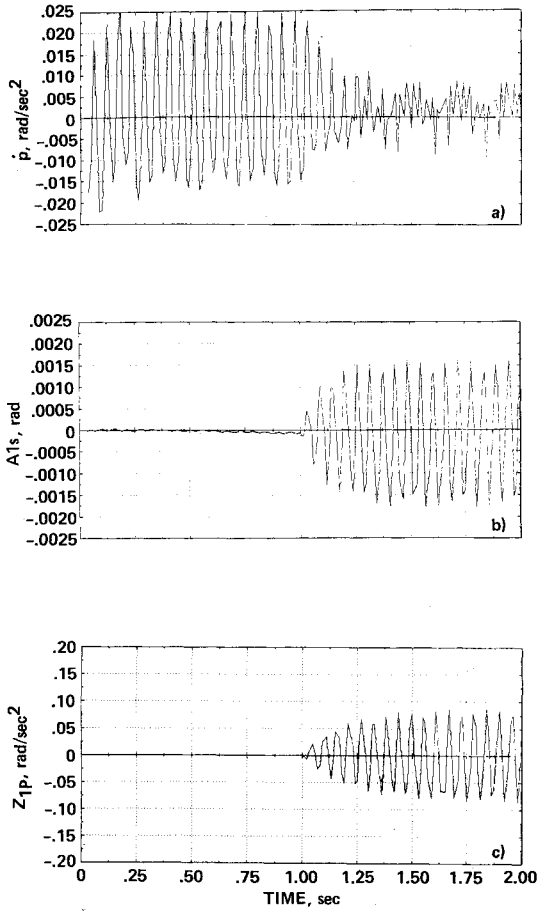

Fig. 4 Roll axis outputs: a) roll acceleration (expanded view), b) lateral swashplate deflection A_{1s}, c) roll vibration sensor output (controller switched at 1 s).

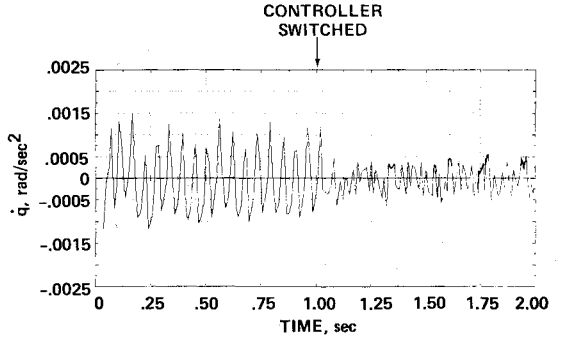

Fig. 5 Pitch acceleration time history (controller switched at 1 s).

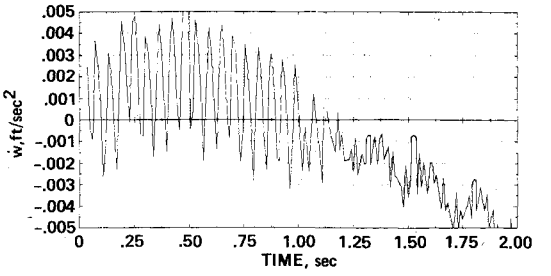

Fig. 6 Vertical acceleration time history (controller switched at 1 s).

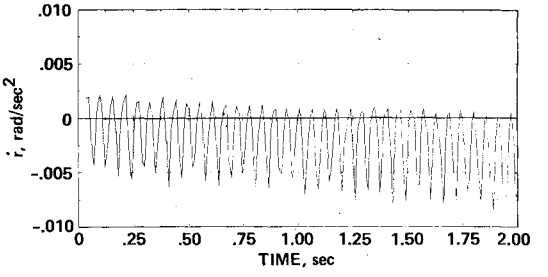

Fig. 7 Yaw acceleration.

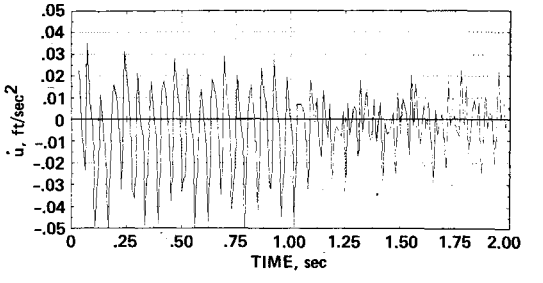

Fig. 8 Longitudinal acceleration.

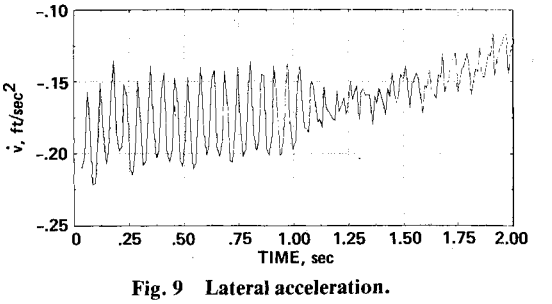

Fig. 9 Lateral acceleration.

originally predominant. The remaining vibrations are at a frequency of 10/rev (2N/rev).

The lateral swashplate deflection (A_{1s}) is shown in Fig. 4b. Some control activity is present prior to the initiation of the vibration controller due to the SAS. The controller locks onto the vibration phase and increases in amplitude to its steady-state value with a time constant of about 0.25 s. Note that the steady-state amplitude is about 0.1 deg. An 18-Hz (5/rev) oscillation at this amplitude is within the capability of most rotorcraft actuators. Significantly higher control requirements are anticipated in forward flight and when blade flexibilities are included.

The output of the roll axis filter is shown in Fig. 4c, and is seen to be very similar to the control output, A_{1s}. This is to be expected since the feedback in the A_{1s} channel is predominantly dependent on the filtered roll acceleration.

The pitch acceleration is shown in Fig. 5. Again, only the 10/rev vibration is visible after the first 0.25 s of vibration-controller activity.

The vertical acceleration is shown in Fig. 6. Again, the 5/rev vibration component is virtually eliminated in 0.25 s, leaving only the 10/rev and higher harmonics. The low-frequency variation in the vertical acceleration occurs because there is no SAS on the collective channel.

The three fuselage accelerations not weighted in the design, $\dot{r}$, $\dot{u}$, and $\dot{v}$, are shown in Figs. 7, 8, and 9, respectively. There is no change in the 5/rev vibration in the yaw channel, $\dot{r}$, since the tail-rotor vibration controller was not implemented. The

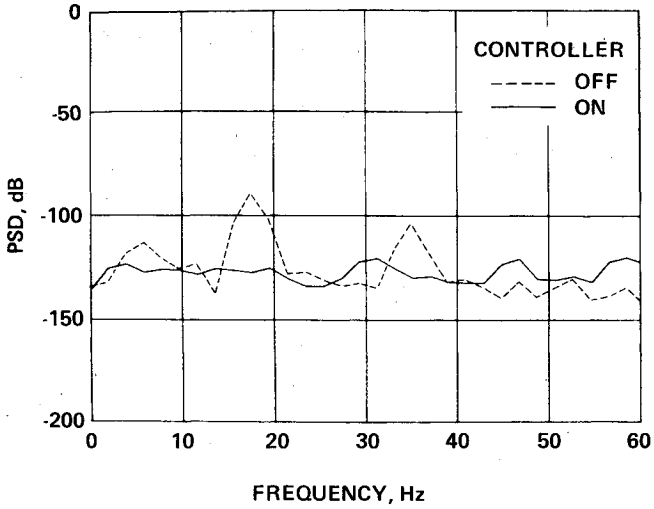

Fig. 10 Pitch acceleration power spectral densities (psd) with and without vibration controller.

longitudinal acceleration $\dot{u}$ has had the 5/rev vibration virtually eliminated, although this was not a design requirement. The lateral acceleration $\dot{v}$ has a considerable reduction in the 5/rev vibration. The implementation of the tail-rotor vibration controller would eliminate the 5/rev vibration in $\dot{v}$ as well as in $\dot{r}$.

Figure 10 compares the open-loop and closed-loop power spectral densities of the pitch acceleration in hover.

Feedback of Filter States Only

Due to the complexity involved in implementing rotor-state feedback, it is desirable to obtain a vibration controller that requires only filtered accelerometer measurements. The linear analysis had indicated that eliminating rotor-state feedback from this design would significantly alter both the rotor and fuselage roots. As an experimental verification, the rotor-state feedback was eliminated from the simulation implementation. The resulting system rapidly went unstable. The roll channel, as predicted by the linear analysis, appeared to precipitate the instability. The low-frequency (regressing) rotor mode involves heavy coupling between rotor states and fuselage roll.[12] Feeding back the roll acceleration without using rotor-state feedback aggravates this coupling to the point of instability. It is interesting to note that the same problem occurred on the RSRA with a mechanical vibration isolator design. A low-pass (2-Hz) filter was required on the SAS roll-rate feedback to prevent the low-frequency rotor mode from driving the SAS unstable in roll. It is anticipated that a similar technique can be utilized to stabilize the active vibration controller without requiring rotor-state feedback.

Robustness

The hover vibration controller was applied to the RSRA nonlinear simulation at 120 knots forward speed. Open-loop and closed-loop power spectra for vertical acceleration and pitch acceleration are shown in Fig. 11. There is significant attenuation in the pitch channel while the other channels are relatively unchanged. Thus, the controller is highly robust.

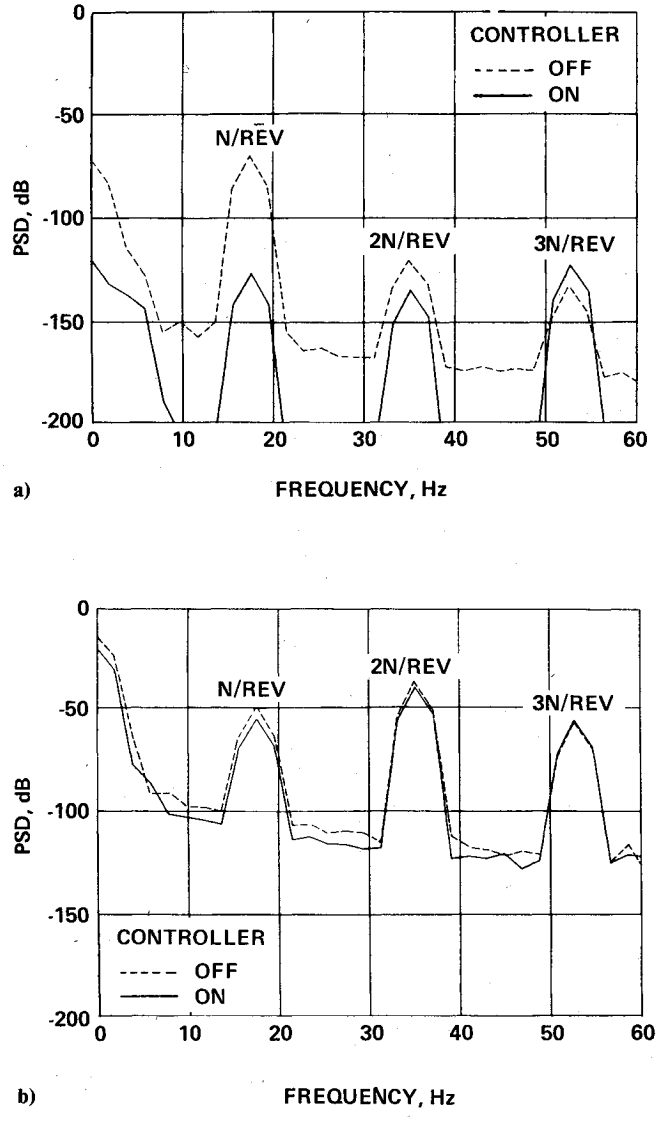

Fig. 11 Power spectral densities at 120 knots forward speed: a) pitch acceleration, b) vertical acceleration.

Conclusions

The study demonstrates the feasibility of using state-feedback-type methods for vibration control in helicopters. Frequency-shaped cost functionals play a key role in this application.

Vibration can be almost completely eliminated at the desired frequency in several axes. Control inputs required to accomplish this reduction appear reasonable. A major attraction of the control law is that it has minimum interaction with the stability augmentation system, allowing for independent designs. Thus, the vibration controller could be used with standard stability augmentation systems. The design is simple, and real-time implementation is unlikely to cause computational problems.

The purpose of this paper is to demonstrate the approach, not attempt to design a vibration controller which can be flown on the vehicle. Extensions are needed to include actuator and sensor dynamics, hysteresis and deadband as well as tail-rotor control. Further, the simulation must include blade structural modes and perhaps fuselage structural dynamics. Care must also be taken to ensure that vibration control at the pilot station does not increase vibration at other helicopter locations to an unacceptable level. Finally, the controller must be simplified. Use of rotor states for feedback is undesirable because of unreliable rotor sensors. State estimator and controller orders can probably be reduced without performance loss. While none of these problems is trivial, we believe satisfactory solutions will be found during the course of current research.

Appendix

F Matrix

	u	w	θ	q	v
$\dot{u}$	−1.19E−02	−1.52E−02	−3.20E+01	−9.11E−01	0
$\dot{w}$	4.44E−02	−4.29E−02	−3.74E+00	−3.43E−01	0
q	0		0	1.00E+00	0
$\dot{q}$	4.58E−04	−1.20E−03	0	0	−2.36E−04
$\dot{v}$	1.80E−02	−8.3E−03	2.64E−01	−2.33E+00	−5.89E−02
p	0	0	0	0	0
$\dot{p}$	8.91E−03	2.88E−03	0	−5.81E−01	−1.78E−02
$\dot{r}$	−5.29E−03	1.00E−03	0	6.01E−02	8.08E−03
$\dot{\beta}_0$	0	0	0	0	0
$\dot{\beta}_{1c}$	0	0	0	0	0
$\dot{\beta}_{1s}$	0	0	0	0	0
$\ddot{\beta}_0$	−1.33E−01	1.24E+00	0	0	0
$\ddot{\beta}_{1c}$	1.82E−01	0	0	−3.71E+01	−2.74E−01
$\ddot{\beta}_{1s}$	−3.49E−01	−8.96E−02	0	3.92E+01	−2.56E−01

	ϕ	p	r	β_0	β_{1c}
$\dot{u}$	0	−1.15E+00	−1.38E−04	3.64E+01	−4.62E+01
$\dot{w}$	2.25E+00	−4.52E−01	3.08E+00	−3.93E+02	−3.40E+00
q	0	0	0	0	
$\dot{q}$	0	2.98E−02	−2.10E−02	8.31E−01	3.07E+00
$\dot{v}$	3.19E+01	−1.44E+00	−1.68E−02	0	−4.88E+01
p	0	1.00E+00	0	0	0
$\dot{p}$	0	−3.46E−01	1.84E−01	0	−2.30E+01
$\dot{r}$	0	−4.14E−03	−2.30E−01	0	3.29E+00
$\dot{\beta}_0$	0	0	0	0	0
$\dot{\beta}_{1c}$	0	0	0	0	0
$\dot{\beta}_{1s}$	0	0	0	0	0
$\ddot{\beta}_0$	0	0	0	−5.97E+02	0
$\ddot{\beta}_{1c}$	0	−4.26E+01	0	0	−3.75E+01
$\ddot{\beta}_{1s}$	0	−4.14E+01	−8.84E+00	0	5.97E+02

	β_{1s}	$\dot{\beta}_0$	$\dot{\beta}_{1c}$	$\dot{\beta}_{1s}$
$\dot{u}$	−5.78E+01	7.40E−01	−2.32E+00	0
$\dot{w}$	−1.36E+01	−1.70E+00	−2.50E−01	−8.46E−02
q	0	0	0	0
$\dot{q}$	1.90E+00	−1.21E−02	9.70E−02	0
$\dot{v}$	5.22E+01	3.17E−01	3.18E−01	2.80E+00
p	0	0	0	0
$\dot{p}$	3.88E+01	−3.42E−03	1.39E−01	1.19E+00
$\dot{r}$	4.65E−01	−2.59E−02	−3.68E−02	1.42E−02
$\dot{\beta}_0$	0	1.00E+00	0	0
$\dot{\beta}_{1c}$	0	0	1.00E+00	0
$\dot{\beta}_{1s}$	0	0	0	1.00E+00
$\ddot{\beta}_0$	0	−3.55E+01	0	0
$\ddot{\beta}_{1c}$	−6.01E+02	0	−2.71E+01	−4.43E+01
$\ddot{\beta}_{1s}$	−6.21E+01	0	4.43E+01	−2.68E+01

G Matrix

	B_{1s}	θ_C	A_{1s}	θ_{TR}
$\dot{u}$	0	5.68E+00	0	0
$\dot{w}$	0	4.04E+01	0	0
q	0	0	0	0
$\dot{q}$	0	−1.12E−01	−1.45E−01	0
$\dot{v}$	0	0	0	1.19E+01
p	0	0	0	0
$\dot{p}$	−1.22E+00	0	−1.81E−01	2.97E+00
$\dot{r}$	−1.61E−01	0	−2.17E−03	−2.71E+00
$\dot{\beta}_0$	0	0	0	0
$\dot{\beta}_{1c}$	0	0	0	0
$\dot{\beta}_{1s}$	0	0	0	0
$\ddot{\beta}_0$	0	6.25E+02	0	0
$\ddot{\beta}_{1c}$	−1.09E+02	0	6.21E+02	0
$\ddot{\beta}_{1s}$	6.19E+02	0	1.07E+02	0

Weighting Factors

$$\frac{1}{\dot{w}_M^2}=0.14 \qquad \frac{1}{\dot{q}_M^2}=400 \qquad \frac{1}{\dot{p}_M^2}=6.25 \qquad \frac{1}{B_{1sM}^2}=1.0 \qquad \frac{1}{\theta^2_{CM}}=1.0 \qquad \frac{1}{A_{1sM}^2}=1.0 \qquad \frac{1}{\theta^2_{TR}}=1.0$$

Feedback Gains

	u	w	θ	q	v
B_{1s}	−7.8201E−05	−6.2726E−05	5.5865E−02	1.0776E−01	2.8279E−04
θ_C	5.4842E−05	−1.5053E−04	−1.2870E−02	−1.3831E−02	1.6282E−05
A_{1s}	−1.3715E−04	1.9270E−04	−2.9556E−02	−4.9164E−02	2.1647E−04
θ_{TR}	−2.3759E−05	1.5101E−05	2.8278E−03	1.0743E−02	−1.4100E−05
	ϕ	p	r	β_0	β_{1c}
B_{1s}	−1.3601E−02	4.5523E−03	−2.0484E−03	9.8201E−03	6.2931E−01
θ_C	3.7968E−03	7.6445E−04	3.0350E−03	−3.9320E−01	1.1650E−02
A_{1s}	−6.7156E−03	4.6391E−04	1.6921E−03	−4.0598E−02	−4.3856E−01
θ_{TR}	−2.0538E−03	−5.1218E−03	−4.8983E−04	1.2019E−03	3.1041E−02
	β_{1s}	$\dot{\beta}_0$	$\dot{\beta}_{1C}$	$\dot{\beta}_{1s}$	z_{1w}
B_{1s}	−7.3695E−01	−2.4775E−04	1.551E−03	−2.8393E−02	−1.2586E−04
θ_C	5.1275E−03	−1.2945E−02	2.3937E−04	3.2438E−04	−1.3479E−03
A_{1s}	−5.5354E−01	1.3842E−03	−2.1398E−02	−6.6786E−03	3.3871E−04
θ_{TR}	−6.7291E−02	1.3709E−04	6.8760E−04	−1.1661E−03	3.9200E−05
	z_{2w}	z_{1q}	z_{2q}	z_{1p}	z_{2p}
B_{1s}	5.9400E−07	−6.3930E−02	−9.7034E−05	2.4222E−02	1.1313E−05
θ_C	−3.5168E−05	−5.5099E−03	1.8569E−04	9.2651E−05	−1.2283E−07
A_{1s}	−1.3126E−06	2.0470E−01	3.5574E−04	7.6105E−03	1.3255E−06
θ_{TR}	−1.5216E−07	1.6799E−02	5.4508E−05	7.3081E−04	−9.4215E−06

References

[1] Laing, E.J., "Army Helicopter and Vibration Survey Methods and Results," *Journal of the American Helicopter Society,* July 1974, pp. 28-38.

[2] Gessow, A. and Myers, G.C., *Aerodynamics of the Helicopter,* Frederick Ungar Publishing Co., 1952.

[3] McCloud, J.L., III and Kretz, M., "Multicyclic Jet Flap Control for Alleviation of Helicopter Blade Stresses and Fuselage Vibration," NASA SP-352, Feb. 1974.

[4] Shaw, J. and Albion, N., "Active Control of the Helicopter Rotor for Vibration Reduction," Preprint No. 80-68, 36th Annual Forum of the American Helicopter Society, May 1980.

[5] McCloud, J.L., III, "Multicyclic Control for Helicopters," Preprint No. 80-70, 36th Annual Forum of the American Helicopter Society, May 1980.

[6] Brown, T.J. and McCloud, J.L., III, "Multicyclic Control of a Helicopter Rotor Considering the Influence of Vibration, Loads, and Control Motion," Preprint No. 80-72, 36th Annual Forum of the American Helicopter Society, May 1980.

[7] Yen, J.G., "Vibration Reduction with Higher Harmonic Blade Feathering for Helicopters with Two-Bladed Teetering and Four-Bladed Hingeless Rotors," Preprint No. 80-69, 36th Annual Forum of the American Helicopter Society, May 1980.

[8] Gupta, N.K., "Frequency-Shaped Cost Functions: Extension of LQG Design Approach," *Journal of Guidance and Control,* Vol. 3, Nov.-Dec. 1980, pp. 529-535.

[9] Bryson, A.E., Jr. and Ho, Y.C., *Applied Optimal Control,* Blaisdell Publishing Co., Waltham, Mass., 1969.

[10] Hohenemser, K.H. and Yin, S.K., "Some Applications of the Method of Multi-Blade Coordinates," *Journal of the American Helicopter Society,* No. 17, July 1972.

[11] Du Val, R.W., "Use of Multiblade Sensors for On-Line Rotor Tip-Path Plane Estimation," *Journal of the American Helicopter Society,* No. 25, Dec. 1980.

[12] Du Val, R.W., and Mackie, D.B., "Identification of a Linear Model of Rotor/Fuselage Dynamics from Nonlinear Simulation Data," Paper No. 60, Sixth European Rotorcraft and Powered Lift Aircraft Forum, Bristol, U.K., Sept. 1980.

[13] Bryson, A.E., Jr. and Hall, W.E., Jr., "Optimal Control and Filter Synthesis by Eigenvector Decomposition," Report No. 436, Dept. of Aeronautics and Astronautics, Stanford University, Stanford, Calif., Nov. 1971.

[14] Houck, J.A., Moore, F.L., Howlett, J.J., Pollock, K.S., and Borwne, M.M., "Rotor Systems Research Aircraft Simulation Mathematical Model," NASA TM-78629, Nov. 1977.